Parallel Fluxgate Magnetometers

Michal Janosek

Abstract This chapter gives a brief overview of parallel fluxgate development, technology and performance. Starting from theoretical background through derivation of fluxgate gating curves, the fluxgate sensor is explained on its typical examples, including sensors with rod-, ring- and race-track core. The effects of geometry, construction and magnetic material treatment on parallel fluxgate noise are discussed in detail–noise levels as low as 2 pT_{rms}·$Hz^{-0.5}$ are possible with state-of-the-art devices. Basic applications of fluxgate magnetometers are given and a quick overview of commercial devices is presented, concluded with recent advances in bulk, miniature, digital and aerospace devices.

1 Background

The parallel fluxgate sensor dates back to the 1930s [1] and most of this early knowledge remains valid until today, although refined by recent findings in the field of sensor noise, core magnetic materials and new principles of signal extraction. Since the early times, the noise level of several nanoteslas has continuously decreased due to evolution in electronic circuits and core materials to units of pT in a 10-Hz bandwidth.

The parallel fluxgate sensor in its simplest form is sketched on Fig. 1 (left)—the time-varying excitation flux Φ_E created in the ferromagnetic core via the excitation field intensity H_E (produced by the excitation coil) and the "measured" field H_M are in *parallel*.

A fluxgate sensor is basically a magnetic field sensor relying on induction law. For its simplest form of Fig. 1 (left), its output voltage U_i present at the pick-up coil terminal P is approximated by the following equation:

$$U_i = -N \cdot S \cdot \left(\frac{dB_E}{dt} + K \cdot \mu_0 \mu_r \cdot \frac{dH_M}{dt} + K \cdot \mu_0 \cdot H_M \frac{d\mu_r}{dt} \right) \qquad (1)$$

M. Janosek (✉)
Department of Measurement, Faculty of Electrical Engineering,
Czech Technical University in Prague, Technicka 2, Prague, Czech Republic
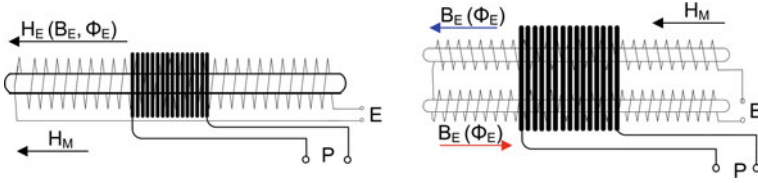e-mail: janosem@fel.cvut.cz

Fig. 1 (*Left*) Simplest parallel fluxgate with a rod-core. (*Right*) Modification with two cores

where H_M is the measured external magnetic field intensity with an eventual time-varying component, B_E is the alternating excitation flux density in the ferromagnetic core due to the excitation field intensity H_E, N is the number of turns of the pick-up coil, S is the core cross-sectional area, μ_0 is the permeability of vacuum and K is a dimension-less coupling coefficient of the core to the field H_M (real core geometry is far from an ellipsoid). The first term in parentheses is present because this simple sensor directly transforms also the excitation flux Φ_E to the pick-up coil, which is the basic disadvantage of this design. The second term is due to the eventually time-varying measured field H_M. However the key principle of a fluxgate sensor is in the last term of the equation—the alternating excitation ("drive") field H_E, which periodically causes the saturation of the magnetic material used in the fluxgate core, modulates the core permeability which has in turn a non-zero time derivative.

The sensor presented in Fig. 1 (left) is however impractical, although sometimes used in low-cost devices. Two cores can be used instead of one core, with each core having an opposite direction of the excitation flux, whereas the pick-up coil shares both of the cores—see Fig. 1 (right). If the core magnetic properties are same for both of them, the first term of Eq. 1—with eventually large disturbing amplitude— is effectively suppressed by the common pick-up coil.

If the measured magnetic field H_M is constant, the second term is also zero and only the third term of Eq. 1 remains as fluxgate output. In agreement with [2] and [3] we can then write for the fluxgate output voltage:

$$U_i(t) = -NS \cdot \mu_0 H_M \cdot \frac{d\mu_r}{dt} \frac{1 - D}{[1 + D(\mu_r - 1)]^2} \tag{2}$$

The "coupling coefficient" K in Eq. 1 was replaced by an equation introducing the dimension-less demagnetization factor D of a ferromagnetic body (fluxgate core).

2   The Physical Model

2.1   *Fluxgate Transfer Function*

The sensor depicted in Fig. 1 (right) can be used for deriving the parallel fluxgate operation principle. As we have two core slabs sharing the same, but opposite-in-direction excitation field H_E (yielding in time-varying $\Phi_E(B_E)$ in the
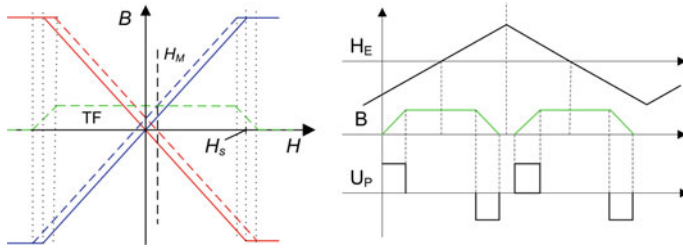
Fig. 2 (*Left*) Transfer function—ideal BH curve. (*Right*) Output voltage derivation with triangular excitation

core), we can draw the corresponding B-H loops for each core (which correspond to one-half of the magnetizing cycle) as seen in Fig. 2 (left). The core B-H loop was simplified to an ideal one with no magnetic hysteresis with H_S standing for the field intensity where it becomes saturated; the red curve corresponds to the lower core of Fig. 1 (right) and the blue one to the upper core. Without any external field H_M (solid curves), if both characteristics are summed, the net change of B during the half excitation cycle is zero. A non-zero external measured field H_M however effectively adds to the exciting field H_E and the resulting B-H loops are shifted (dashed curve). After their summation for both cores we obtain an effective "B-H transfer function" TF or "gating-function": the flux in the core (core flux density) is being periodically gated by the excitation field, the threshold is set by the H_S value and size of the external field H_M.

Now considering a triangular waveform of the excitation field H_E as in Fig. 2 (right) and applying the transfer function TF to it, we can derive the output voltage at the pick-up coil U_P as the core flux density B derivative. It can be seen that the output voltage is at twice the frequency of H_E and its magnitude and also phase lag would be proportional to the measured field H_M.

When taking into account also the material hysteresis, the transfer function will modify accordingly [2] as shown in Fig. 3 (left). However the approach-to-saturation
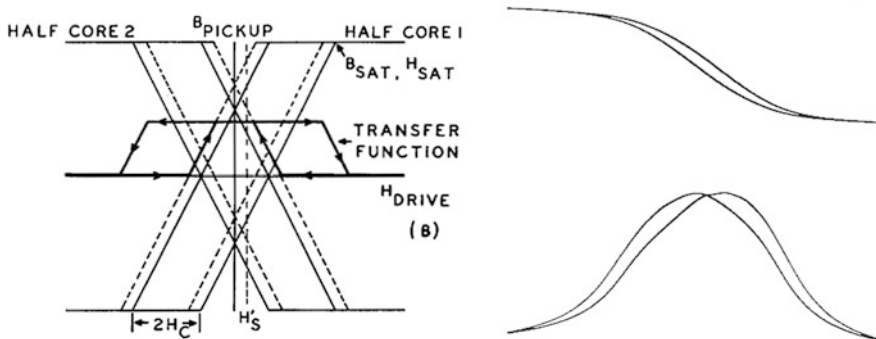

Fig. 3 (*Left*) Gating function with hysteresis from [2]. (*Right*) Real gating function from [3]

shown in Figs. 2 (right) and 3 (left) is not realistic—in Fig. 3 (right) a real BH loop and the corresponding gating function are shown.

An analytical approach to derive the fluxgate output signal was done as early in 1936 [1] and since then many improvements in the model were achieved, also by applying a Fourier-transform to the pulse-train shown in Fig. 2 (right), see [2–5]. However the original Aschenbrenner's approach is shown below since it gives a simple analytical demonstration of the origin of second harmonic in the fluxgate output signal.

Let's have a very simple approximation of the BH magnetizing curve [1], assuming the coefficients $a > 0$, $b > 0$:

$$B = a \cdot H - b \cdot H^3 \tag{3}$$

At each of the magnetic cores of Fig. 1 (right), the measured field H_M and the harmonic excitation field $H_E = A \sin \omega t$ are summed up:

$$H_{1,2} = H_M \pm H_E = H_M \pm A \sin \omega t \tag{4}$$

The corresponding flux density B in each of the two cores is then expressed using Eq. 3:

$$B_{1,2} = a(H_M \pm A \sin \omega t) - b(H_M \pm A \sin \omega t)^3 \tag{5}$$

$$
\begin{aligned}
B_{1,2} = {} & a \cdot H_M - b \cdot H_M^3 - \frac{3}{2} b \cdot A^2 \cdot H_M \\
& \pm \left(a \cdot A - 3b \cdot A \cdot H_M^2 - \frac{3}{4} b \cdot A^3 \right) \sin \omega t \\
& + \frac{3}{2} b \cdot A^2 H_M \cos 2\omega t \ \pm \ \frac{1}{4} b \cdot A^3 \sin 3\omega t
\end{aligned}
\tag{6}
$$

If both cores are of equal cross-section S, the flux is then added by the means of common pick-up coil and after summing we get the remaining terms:

$$
\begin{aligned}
\Phi &= S \cdot (B_1 + B_2) \\
&= 2S \cdot \left(a \cdot H_M - b \cdot H_M^3 - \frac{3}{2} b \cdot A^2 \cdot H_M + \frac{3}{2} b \cdot A^2 H_M \cos 2\omega t \right)
\end{aligned}
\tag{7}
$$

The only time-varying component is at the second harmonic of excitation field frequency:

$$\Phi(t) = 3S \cdot b \cdot A^2 \cdot H_M \cos 2\omega t \tag{8}$$

Again we see that the time-varying output is at the second harmonics of the excitation frequency and its amplitude is directly proportional to the measured, static field H_M. If H_M was time-varying, there would be also a signal at the fundamental frequency. In reality, however, also higher-order even harmonics are
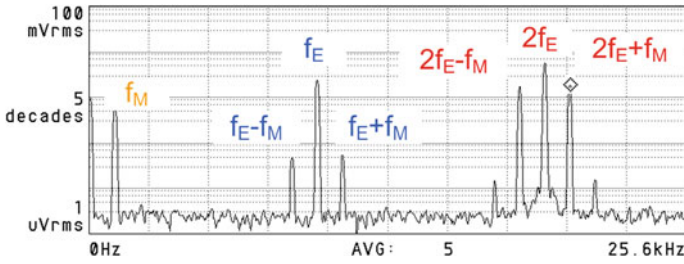
Fig. 4 The ac-driven fluxgate output spectrum

present, due to the nature of the B-H loop (hysteresis, approach to saturation) and non-sinusoidal excitation waveforms with higher harmonics. These effects are taken into account by the modern fluxgate models [2–5].

2.2 The Fluxgate as a Modulator

A real-world output of a fluxgate sensing a field H_M with both ac and dc component can be seen in Fig. 4—f_M is the frequency of alternating component and f_E is the excitation signal frequency. Signal at f_E which is present due to non-ideal symmetry of the sensor: i.e. the complementary terms of Eq. 6 are not exactly of the same amplitude and phase, so they do not subtract completely. The signal exactly at the second harmonics $2f_E$ is due to the dc component of H_M. The measured field H_M is thus modulated on the excitation second harmonics. However due to the non-ideal symmetry of the sensor, it appears modulated also on the fundamental excitation frequency f_E. This applies not only to dc but also to the ac signal at f_M, which appears at $2f_E \pm f_M$ and $f_E \pm f_M$.

It can be concluded from the spectrum in Fig. 4 that an alternating signal is amplitude-modulated with a carrier on the 2nd harmonics of fluxgate excitation frequency, while the amplitude of the carrier is proportional to the dc component of the signal. This can be proven by substituting $H_M + B \cdot \cos(\psi t)$ for H_M in Eq. 8. If the excitation field would contain higher harmonics, there will be also higher modulation harmonics present in the spectra and the higher-order even harmonics will contain the information about the measured magnetic field.

3 The Parallel Fluxgate Noise

The fluxgate noise generally exhibits a $1/f$ behavior with a noise amplitude spectral density $(ASD = \sqrt{PSD})$ as low as 2–3 pT$_{rms}$ Hz$^{-0.5}$ @ 1 Hz, typically ~ 10 pT$_{rms}$ Hz$^{-0.5}$. However, the noise due to the magnetometer electronic circuitry mostly limits at least the white noise floor (amplifier noise, detector phase

noise etc.), which makes measuring the fluxgate noise difficult and subject to large statistical errors.

The actual fluxgate noise can be related to three effects—stochastic behavior of the Barkhausen noise, or better explained as irreversible rotation and domain wall-displacement process during the fluxgate magnetizing cycle [6–8], thermal white noise [9] and an excessive, small-scale noise [10] which is seen at many fluxgates with supposedly low Barkhausen noise. The latter is believed to originate from inhomogeneous, stochastic magnetoelastic coupling of the non-zero magnetostrictive core to external stresses [11] rather to magnetostrictive movement itself [12]. The white noise of the pick-up coil does not have much influence, since although with increasing coil turns resistance increases but also the voltage sensitivity increases.

An important factor is the coupling of the "internal" fluxgate core noise to the actual sensor noise via the core demagnetization factor D. It can be written [13]:

$$B_{SensorNoise} \cong D B_{CoreNoise} \tag{9}$$

For Barkhausen noise, it was shown by van Bree [6], that minimum detectable signal H_0, which is equal to noise for SNR 0 dB, can be expressed as

$$H_{0(Bh)} = \frac{B_S}{\mu_0 \mu_r} \sqrt{\frac{\tau}{N_B \cdot t_m}} \tag{10}$$

where τ is the magnetization period lower limit (inverse of excitation frequency), t_m is the measurement time, B_s is the saturation flux density and N_B is the density of Barkhausen volumes after Bittel and Storm [8]. For the lower limit of $N_B = 10^4$, $\tau = 10^{-6}$ s, $t_m = 1$ s and $\mu_r = 8000$ [6], H_0 yields in about 2×10^{-6} A/m (2 pT in air) which corresponds to the state-of-the art materials with low Barkhausen noise [14].

The white noise is usually estimated according to the (thermal) fluctuating current in the core: the component perpendicular to the core axis creates magnetic field noise, which couples to the pick-up coil [9]—Eq. 11.

$$I_{core} \left[\frac{A_{rms}}{\sqrt{Hz}} \right] = \sqrt{\frac{4kT}{R_{core}}} \tag{11}$$

This "white-noise current" is also present at the 2nd harmonics. In this case, Eq. 11 should take into account the core "effective resistance" Re{Z} due to the skin-effect. However, since now we are considering only the correlated component at the 2nd harmonics, the noise couples to the pick-up coil only by the (low) residual transformer term of Eq. 1.

For usual core volumes, the predicted white noise is at least an order of magnitude below the observed fluxgate noise: for the race-track sensor [9] with 2 pT$_{rms}$ Hz$^{-0.5}$ @ 1 Hz the white noise was about 0.39 pT$_{rms}$ Hz$^{-0.5}$. In a single-domain fluxgate [14], white noise about 50 fT was reported utilizing a cross-spectral measurement technique.
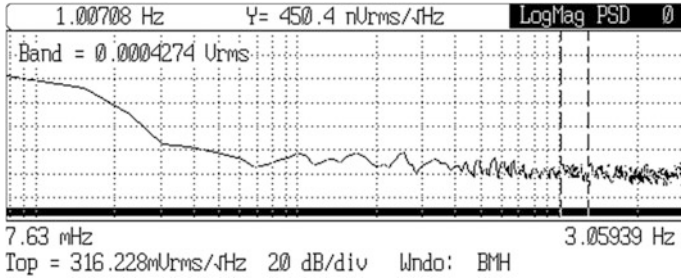
Fig. 5 Typical fluxgate magnetometer noise (TFM100G2, 100 kV/T, SR770)

A typical fluxgate noise is depicted below in Fig. 5—the low-noise TFM100G2 magnetometer of Billingsley A&D exhibits approximately 1/f character between 10 and 300 mHz and almost white response starting at 1 Hz with ASD about 4.5 pT$_{rms}$ Hz$^{-0.5}$, which is a limit of the electronics, not the sensor itself.

4 Fluxgate Geometry and Construction

The core geometry plays an important role in constructing the parallel fluxgate sensor: the sensors can be roughly divided in two families according to core geometry. Rod sensors utilize cores with open magnetic path, ring-cores and race-tracks use closed path cores.

4.1 Rod Sensors

The design using two magnetic rods as in Fig. 1 (right) with a common pick-up coil was used already in 1936 by Aschenbrenner and it is also often referred as "Förster configuration" after the researcher and manufacturer F. Förster who utilized it. An example is in Fig. 6 with two thin Permalloy cores in glass tubes, on top of which the excitation coils are wound [compare to Fig. 1 (right)]. Alternatively, there can be two pick-up coils anti-serially connected which would be wound directly on the excitation coils—the so-called "Vacquier configuration" patented by V. Vacquier in 1941.

The advantage of rod sensors is low demagnetization factor due to the favorable ratio of cross-section and length which is in the direction of measured field. The disadvantage is that due to the open magnetic path the level of saturation is different across the core length, causing problems with sensor offset. The pick-up coil is then placed not to cover the noisy, unsaturated core ends [15].

Fig. 6 The rod fluxgate
(Förster type) before
assembly

4.2 Ring-Core and Race-Track

As stated previously, the construction of a parallel fluxgate should assure good symmetry to suppress unwanted excitation signal and also possibly to reduce the noise by strong excitation field: this can be obtained with a closed-path magnetic core. In terms of Eq. 4, the sensor can be virtually divided to two "core halves" with opposite excitation field direction—see Fig. 7. The key advantage of the ring-core [Fig. 7 (left)] is the possibility to rotate the pick-up coil in order to obtain best suppression of the residual excitation signal (due to transformer term in Eq. 1). Its disadvantage is the relatively large demagnetization factor decreasing its sensitivity when compared to the rod designs. To decrease the demagnetization factor, a sensor with an oval, race-track shape of ferromagnetic core [Fig. 7 (right)] is often designed. However its balance is not easily achieved as for ring-cores.

4.3 Bulk Sensors and Micro-fluxgates

The classical parallel fluxgate is a bulk-type, i.e. it uses magnetic core material from magnetic tape/wire or even a bulk material with wire-wound excitation and pick-up
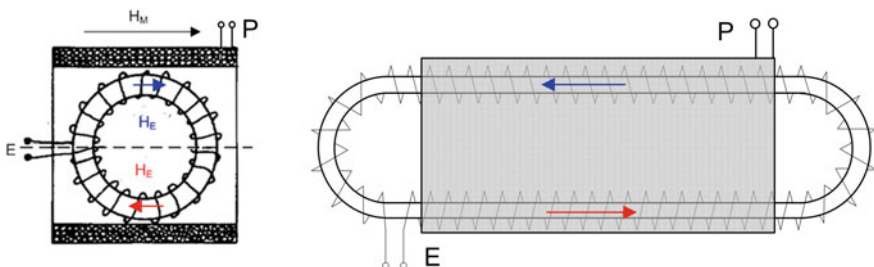

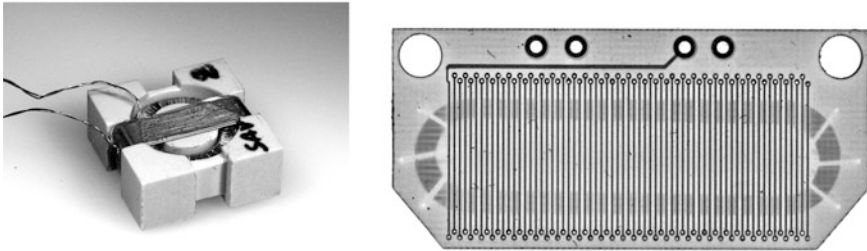**Fig. 7** (*Left*) The ring-core with H_E in "core halves." (*Right*) The race-track sensor

Fig. 8 (*Left*) The real 12-mm-dia ring-core is a typical bulk sensor. (*Right*) The 30-mm long race-track is created in PCB technology

coils. The final core shape in larger sensors is then obtained by winding the magnetic tape [16] or the annealed wire [14] to a core holder [Fig. 8 (left)]; a stress-free alternative is etching or arc-cutting the final core shape from a wide magnetic tape [17]. The advantage of bulk fluxgates is their high sensitivity due to large cross-section and high number of pick-up coil turns, and also low demagnetization factor achievable with long sensors. Disadvantages are their cost and mass which start to be a limiting factor even in aerospace applications where bulk fluxgates still find use [18]. An approach to at least simplify the manufacturing design has been done with PCB fluxgate sensors [19]—Fig. 8 (right), however despite the comparable size their parameters are inferior to that of classical ones mostly due to residual stresses after manufacturing (bonding of the ferromagnetic core) [20]. Electroplated ring-core fluxgates on PCB substrates have been presented by Butta [11], the thin layer was advantageous for high-frequency performance of the sensor.

Fluxgate micro-sensors appear since the end of 1980s. Their limitation is mostly very low sensitivity, resulting in 1-Hz ASD about 1 $nT_{rms} Hz^{-0.5}$ even when using excitation frequencies in the range of 1 MHz. The way of magnetic core manufacturing is often limited by desired sensor design: the need for solenoid coils and integrating the core mostly leads to MEMS devices; CMOS devices rely on flat-coils with worse coupling to the ferromagnetic core. An integrated micro-sensor core would require electrolytic deposition [21], integrating the etched tape [22] or sputtering [23].

5 Fluxgate Noise and Ferromagnetic Core

During the 80 years of fluxgate development, it has been finally understood that the core parameters are the key for a low-noise, high-sensitivity sensor [14, 16, 24]. The ferromagnetic core for a parallel fluxgate should fulfill several requirements arising from Eq. 2 and the principle of operation; these requirements affect several different parameters. Table 1 shows the list of required parameters and the most affected property.

Table 1 Influence of core parameter on fluxgate performance

Core parameter	Primary effect	Secondary
Low demagnetization factor	Sensitivity	Noise
Low Barkhausen noise	Noise	–
Low magnetostriction, low applied stresses	Offset	Noise
High permeability	Sensitivity	Power consump.
Approach to saturation	Noise	–
Thickness/resistivity	Losses	High f operation
Curie temperature	Operating range	Noise

5.1 Core Shape—Demagnetization Factor

Keeping the core demagnetization factor D low (lowest for rod-type sensors) not only allows for high sensitivity to external fields (Eq. 2) but also provides better ratio to the "core noise"—see Eq. 9. Thus a common practice to decrease sensor noise, if the limits of improving the magnetic material are reached, is to decrease D.

The demagnetization factor of a ring-core with a diameter d and effective core thickness T was estimated from a number of calculations and measurements [13]:

$$D \cong 0.223\ (T/d) \tag{12}$$

However it is relatively easy to model D it in today's FEM packages for arbitrary shapes. In Fig. 9 (left), the demagnetization factor of a 10-mm ring-core was calculated using ANSYS and also FLUX 3D software. The ferromagnetic tape was 20 μm thick and 2.6 mm wide with μ_r = 15,000. The resulting demagnetization factors for 5, 18 and 46 tape turns agree well with that calculated by Eq. 12. The relation between fluxgate noise and the demagnetizing factor due to Eq. 9 as proposed by Primdahl was later proved for large ring-core sensors [25]—the typical dependence is depicted in Fig. 9 (right). The increased noise at very low D values appears due to the fact that a smaller cross-section causes loss of SNR, assuming the existence of external induced noise coherent to the 2nd harmonic.
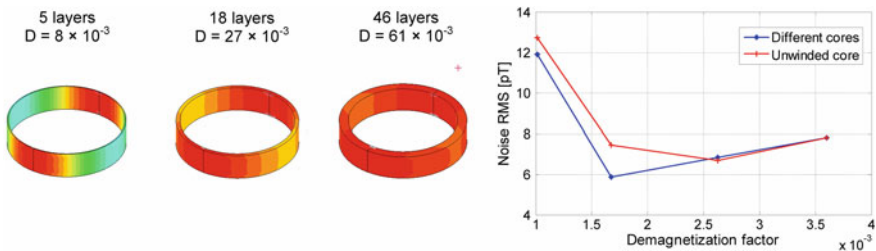

Fig. 9 (*Left*) Calculated demag. factor D of 10-mm ring [25]. (*Right*) Noise versus D for 50-mm rings

5.2 Core Material and Processing

Historically, the core materials were iron [1] or ferrites [3]. Later crystalline Ni-Fe started to be used in the form of tapes or rods ending up with specially annealed Molybdenum-Permalloy tapes [26] which are still being utilized in space research [18]. With these crystalline materials, the cores have to be annealed with the material already in its final shape. The inherent advantage of Permalloys is their high Curie temperature, allowing for high temperature operation, however special care of the material composition is necessary to achieve near-zero magnetostriction. Since 1980s there is a widespread use of amorphous materials, mostly in form of thin tapes and wires, which do not require hydrogen annealing in the final form and are less mechanically sensitive. Cobalt-based amorphous materials tend to be the best candidates for the sensors [16] however also in this case sufficient annealing process is necessary to obtain the same or better performance than the heritage Mo-Py cores.

Low Barkhausen noise is generally obtained in materials with very low area of the hysteresis loop with prevalent domain-wall rotations rather than domain-wall movements. This is achieved usually by perpendicular-field or stress annealing of the magnetic material to introduce perpendicular anisotropy, thus promoting domain-wall motion rather than sudden jumps due to the domain wall movement [16, 24]. Influence of Curie temperature on noise was studied by Shirae for various amorphous compositions [27]—a strong correlation between low Curie temperature and low fluxgate noise was found.

Since the end of the 20th century, nanocrystalline materials receive great attention because of their good thermal stability and stable phase, which makes them suitable for down-hole drilling [28] and possibly in space research. However their disadvantage is the relatively high saturation induction, requiring high excitation power and higher noise even after proper annealing.

6 The Feedback Compensated Magnetometer

The diagram of a typical feedback-compensated fluxgate magnetometer is on Fig. 10. The magnetometer usually uses feedback in order to achieve better stability and linearity of the device: the measured field is zeroed by an artificial field with opposite sign, created either by a coil shared for also for voltage pick-up, or by a separate compensating coil. The standard means of achieving the compensation field is using an integrating regulator feeding a feedback resistor or driving an active current source.

Alternatively, for full-vector magnetometers, the feedback coils can be integrated to a triaxial coil system where the orthogonal sensor triplet is placed, assuring high homogeneity of the compensating field and suppressing the parasitic sensitivity to perpendicular fields [30]. Also the mutual influence of feedback fields of the closely located sensors is suppressed.
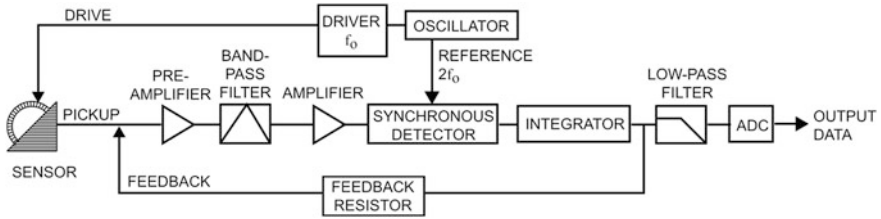
Fig. 10 The feedback compensated magnetometer from [29]

The sensitivity of the compensated magnetometer depends—by its operating principle—only on the coil constant of the compensating coil. The open-loop sensitivity (given by number of pick-up coil turns, core volume, demagnetization factor, permeability, drive waveform etc.) then affects the noise or resolution of the magnetometer, which ideally remains the same as in open-loop. The magnetometer linearity can be in tens of ppm and its gain stability better than 20 ppm/K, which in a good design is limited by the thermal expansion of the compensating coil (and its support) rather than by the electronics itself [30]. However, even for best magnetometers, the real-world limiting factor affecting the magnetometer resolution is the sensor offset and its temperature drift, which are not suppressed by the feedback loop. The offset is frequently caused by the non-ideal excitation waveform, which may contain parasitic signal at second-harmonic, which is not suppressed due to finite balance of the pick-up coil and the two ferromagnetic cores (or core halves). The core itself can be further affected by perming (i.e. large field shock, which causes change in the core remanence). Another significant contribution to the offset is the core in-homogeneity and its magnetostrictive coupling to inhomogeneous external stresses [12]; much lower contribution is to be expected from the electronics, such as amplifier non-linearity and detector offset. A detailed study of influence of the electronics on magnetometer parameters was presented by Piel [31].

6.1 Magnetometer Electronics

6.1.1 Analog

Signal processing of the pick-up voltage in an analog design normally uses an appropriate circuit for phase-sensitivite, dc-coupled down-conversion of the modulated signal on 2nd excitation harmonics (synchronous detector—phase sensitive detector/mixer)—this is done mainly when the fluxgate output signal at the pickup-coil can be "tuned" by a resonant capacitor to suppress higher-order even harmonics. Another detection possibility is "in time-domain" by integrating the output voltage [20]. Alternatively, it is possible to "short-circuit" the output

fluxgate terminals by a current-to-voltage converter and then process the pulse-like signal proportional to the gated flux [32]. Other techniques use the information of time-lag of the fluxgate output pulses in a special detector circuit [33, 34].

After the detector circuit, the feedback regulator (integrator) stage assures the feedback current, which is sensed, filtered and its value processed in an A/D converter. The fluxgate excitation (oscillator + driver in Fig. 10) in reality does not use sine-wave or triangular excitation signals, as shown in the derivation of the fluxgate output function. In order to save power, either pulse excitation using H-bridge is used [20] or the excitation circuit is "tuned", i.e. the excitation waveform is generated by switches and the non-linear inductance of the excitation circuit is tuned to serial-parallel resonance obtaining sharp excitation peaks. In that way the losses in the excitation circuit can be lowered only to ohmic losses of the excitation winding, moreover it was shown that the amplitude of the excitation signal has an inverse proportional effect on sensor noise [35].

6.1.2 Digital

Early digital magnetometer designs ended up with higher noise than the analog fluxgate with its D/A converter, however at least in space applications the trend is to integrate the electronics to an ASIC which can be further radiation-hardened for aerospace applications. The signal path historically utilized appropriate analog-to-digital converters and signal processing in DSP/FPGA together with D/A converters for feedback [36].

Recently, the fluxgate sensor was successfully integrated in an higher-order delta-sigma feedback loop electronics [37]—the power consumption of the corresponding ASIC (Fig. 11), which carries out the signal demodulation, feedback compensation and digital readout, was only 60 mW and the magnetometer performance was at least equivalent to 20-bit+ analog magnetometers with delta-sigma ADC's [38].

7 Applications

The first fluxgate applications appeared in the field of geomagnetic studies [1] and later also in the military or defense sector—"flux-valves" served for detection of ships or submarines [39]. After WWII, fluxgates have been extensively used in compasses/gyrocompasses in shipping and aviation [40], they have also found their use in attitude control of rockets or missiles and later they started to be used also on satellites [41]. Fluxgate sensors have been used in planetary studies since the early Apollo missions [26] and remained in their form almost unchanged—despite improved electronics—in the aerospace segment up to today [18]. Geophysical prospecting used aircraft-mounted fluxgates from the very beginning, and since
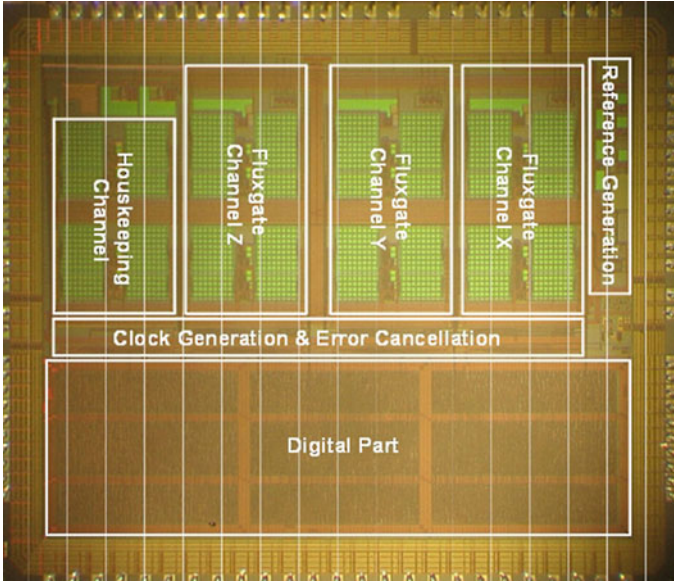
Fig. 11 Microphotograph of the MFA fluxgate ASIC. Reprinted from [37] with kind permission of the author

1980s, sufficient methods appeared to precisely calibrate the sensors, which allowed their use even onboard spacecraft for satellite-based geophysical research [42, 43].

One of the most common applications of a fluxgate for ground-based surveys is a magnetic gradiometer, consisting mostly of two aligned uniaxial sensors or two triaxial sensor heads. For a single-axis gradiometer, the estimated gradient dB_x/dx would be an approximation from two sensor readings B_{x1} and B_{x2} in a distance d:

$$\frac{\partial B_x}{\partial x} = \lim_{d \to 0} \frac{B_{x1} - B_{x2}}{(x_1 - x_2)} \cong \frac{B_{x1} - B_{x2}}{d} = \frac{\Delta B_x}{\Delta x} \tag{13}$$

Equation 13 implies the high requirements on individual fluxgate sensor noise if the sensor spacing d should be reasonable, i.e. below 1 m. Metal or UXO (Unexploded Ordnance) detectors using fluxgate find application also in underwater mine-hunting [44] and because of the cheap computational power now available, they are even constructed as full-tensor gradiometers which allow for localizing the magnetic dipole.

There also exist fields in biomedicine where fluxgate (gradiometers) have found their application: magneto-relaxometry (MRX) [45] and magneto-pneumography (MPG) [46]. Parallel fluxgate—or at least their principle—are also used for contact-less, precise dc/ac current measurements [34, 47].

8 Commercial Fluxgates

8.1 Magnetometers

There are actually very few suppliers who would sell good-quality fluxgate sensors separately—complete magnetometers are mostly offered. One common configuration is a triaxial magnetometer with analog outputs, the transfer constant (sensitivity) is mostly 100,000 V/T. Such instruments are for example of TFM100G2 (Billingsley Aerospace & Defense, USA), MAG03 (Bartington, UK), FGM3D (Sensys, Germany), TAM-1 or LEMI 024 of Laboratory of Electromagnetic Innovations (Lviv, Ukraine). Digitalization of these analog instrument outputs is upon the user or a special hardware is available from the manufacturers. Magnetometers which feature digital outputs (d-) are e.g. the Billingsley DFMG24, LEMI-029, the 3-axis magnetometer of Förster, Germany and FVM-400 of MEDA, USA. Table 2 summarizes most important parameters of the mentioned magnetometers.

8.2 Fluxgate Gradiometers/UXO Detectors

Table. 3 shows parameters of several commercially available gradiometers (UXO detectors), as manufactured by Schonsted (WV, USA), Förster (Germany), Geoscan (UK) or Bartington (UK). Although the gradiometer noise can be a parameter for selecting the best instrument, in reality, the gradiometer resolution is given by gradiometer calibration (astatization) which limits its real-world performance: the large, homogeneous Earth's field will cause false response unless the gradiometer is perfectly aligned or calibrated.

Table 2 Parameters of several commercial magnetometers

Magnetometer type	Range ($\pm\mu T$)	Noise (1 Hz) ($pT_{rms}/\sqrt{Hz}$)	3-dB BW (kHz)	Offset drift (nT/K)	Power (W)
TFM100G2	100	5–10	0.5/4	0.6	0.4
MAG03	70	6–10–20	3	0.1	0.5
FGM3D	100	15	2	0.3	0.6
LEMI 024	80	6	0.5	N/A	0.35
d—FVM-400	100	N/A	0.05/0.1	N/A	0.55
d—DFMG24	65	20	0.05	0.6	0.75
d—LEMI-029	78	6 (w/comp)	0.18	N/A	0.5
d—Förster 3-Axis	100	35	1	1	3.6

Table 3 Parameters of several commercial gradiometers

Gradiometer type	Base (m)	Resolution (nT/m)	Mass (kg)	Power (W)
Schonsted GA52Cx	0.5	N/A	1.1	0.2
Förster Ferex (0.6 m, w/logger)	0.65	1.5	4.9	2
Geoscan FM256	0.5	2	2.5	0.5
Bartington GRAD601 (w/logger)	1	<1	1.3	1.1

9 State of the Art—Recent Results

Recent achievements, either in the field of sensors, or in final magnetometers/gradiometers, are mainly determined by improving the ferromagnetic core material and sensing technologies.

9.1 Bulk Sensors, Magnetometers and Gradiometers

A fluxgate magnetometer with high-temperature rating of +250 °C was presented by Rühmer [28], the sensor core utilized nanocrystalline Vitroperm VP800R. Similar study was done before by Nishio [48] for Mercury exploration satellite, where the sensor characteristics were measured in −160 to +200 °C range.

Noise of a miniature, 10-mm diameter amorphous ring-core fluxgate was shown to decrease by field-annealing down to 6 pT_{rms} $Hz^{-0.5}$ @ 1 Hz [24] which is comparable to the state-of-the-art 17-mm aerospace sensors of the Danish Technical University [30] and also crystalline Mo-Py sensors used by the Geophysics and Extraterrestrial Physics group of the Technical University Braunschweig, Germany [18]. By decreasing the demagnetization factor by optimizing core geometry and the core cross-section of large ring-cores, it was shown by the author that 2 pT_{rms} $Hz^{-0.5}$ can be achieved even with an as-cast tape [25]. The problem with low sensitivity of miniature fluxgates was addressed by Jeng [49] who showed an improvement of $2\times$ in the miniature magnetometer noise by using information from multiple even harmonics.

A study relating the magnetostrictive coupling of fluxgate core to external stresses with fluxgate noise was done by Butta [11]. The origin of the fluxgate offset was recently studied by Ripka [12] and it is—together with excessive noise—believed to be the effect of (local) magnetoelastic coupling, if other sources like perming or offset due to electronics are excluded.

In the field of gradiometers, the state-of-the art in axial devices is still the construction of DTU [50] with two triaxial vectorially-compensated heads, separated by 60 cm: the achieved resolution was 0.1 nT_{rms} m^{-1}. An underwater "real-time-tracking autonomous vehicle" developed at Naval Surface Warfare

Center, FL, USA [51] exhibited noise below 0.3 nT m^{-1} Hz$^{-0.5}$ @ 1 Hz, after compensating the vehicle noise. Recently, a similar full-tensor gradiometer vectorially compensated by a compact-spherical-coil was shown by Sui [52], which has the perspective to further decrease the gradiometer error and increase its sensitivity due to common compensation of the homogeneous field for all the 4 × 3 sensors.

9.2 Micro-fluxgates

A low-noise MEMS microfluxgate with nanocrystalline core embedded by chemical etching and with 3D solenoid coils was presented by Lei [22]. The sensor size was 6 × 5 mm^2 and the noise was as low as 0.5 nT Hz$^{-0.5}$ @ 1 Hz. Texas Instruments has recently published a CMOS-integrated Förster-type micro-fluxgate for contactless current sensing using a gradiometric arrangement [53]. It is also intended for closed-loop current measurement, where it replaces the common Hall-probe in the yoke gap. Its microphotograph is in Fig. 12: the Förster sensor is shown together with the excitation and signal-processing electronics. The microfluxgate operates at 1 MHz, achieves 0.2 mA resolution and was released as "DRV421". Recently, also a standalone micro-fluxgate in a 4 × 4 mm^2 QFN chip was released, with a noise of 1.5 nT Hz$^{-0.5}$ @ 1 kHz [54].
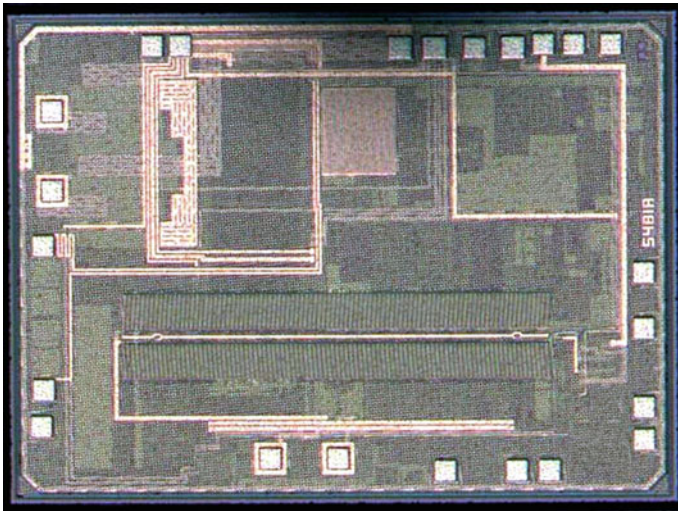

Fig. 12 The CMOS integrated Förster fluxgate, reproduced with kind permission of Texas Instruments, Inc
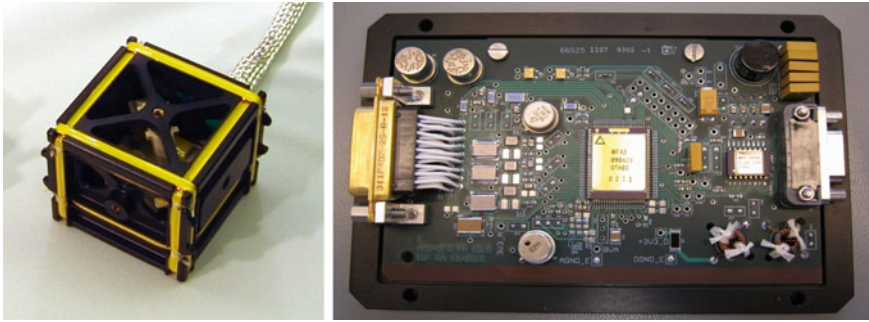
Fig. 13 The magnetic sensor and digital electronics of MMM mission (flight model, not to scale)
—reproduced with kind permission of Werner Magnes /IWF Graz

9.3 Space Applications

An offset-reduction technique proposed by DTU for satellite missions [55] allowed
to decrease offset drift of the heritage analog magnetometer design [30] to ± 0.5 nT
in a 73 °C range—the temperature changes in the excitation resonant circuit were
compensated by an adaptive control of the detector phase. The digital-detection
delta-sigma magnetometer of the THEMIS mission (launched 2007, still active)
achieved offset stability of approximately 0.05 nT/K in the −55 to 60 °C temper-
ature range [18]. These parameters became the state-of-the art in space fluxgate
magnetometers.

The recently successful ROSETTA Explorer and its lander PHILAE used
fluxgate magnetometers; the instrument noise was about 22 pT_{rms} in 0.1–10 Hz
band [56]. The SWARM multi-satellite mission, launched in 2013, carries onboard
several atomic magnetometers and also traditional fluxgates from DTU Denmark,
and is now producing valuable data for a new Earth's field model and other geo-
physical observations [43]. A similar NASA "Magnetospheric Multiscale Mission"
was launched in March 2015; the spacecraft carries analog and also
delta-sigma-loop-integrated magnetometers with custom ASIC developed at the
IWF Graz, Austria [37]—see Fig. 13. Multiple magnetometers have been used and
large effort was made to achieve magnetic cleanliness [38].

References

1. H. Aschenbrenner, G. Goubau, Eine Anordnung zur Registrierung rascher magnetischer Störungen. Hochfrequenztechnik und Elektroakustik **47**(6), 177–181 (1936)
2. D.I. Gordon, R.H. Lundsten, R. Chiarodo, Factors affecting the sensitivity of gamma-level ring-core magnetometers. IEEE Trans. Magn. **1**(4), 330–337 (1965)
3. F Primdahl, The fluxgate mechanism, part I: the gating curves of parallel and orthogonal fluxgates. IEEE Trans. Magn. **6**(2), 376–383 (1970)

4. J.R. Burger, The theoretical output of a ring core fluxgate sensor. IEEE Trans. Magn. **8**(4), 791–796 (1972)
5. A.L. Geiler et al., A quantitative model for the nonlinear response of fluxgate magnetometers. J. Appl. Phys. **99**(8), 08B316 (2006)
6. J.L.M.J. van Bree, J.A. Poulis, F.N. Hooge, Barkhausen noise in fluxgate magnetometers. Appl. Sci. Res. **29**(1), 59–68 (1974)
7. M. Tejedor, B. Hernando, M.L. Sánchez, Reversible permeability for perpendicularly superposed induction in metallic glasses for fluxgate sensors. J. Magn. Magn. Mater. **133**(1), 338–341 (1994)
8. H. Bittel, L. Storm, *Rauschen. Eine Einfuehrung zum Verstaendnis elektrischer Schwankungserscheinungen*. (Springer, Berlin, 1971) (1)
9. C. Hinnrichs et al., Dependence of sensitivity and noise of fluxgate sensors on racetrack geometry. IEEE Trans. Magn. **37**(4), 1983–1985 (2001)
10. D. Scouten, Sensor noise in low-level flux-gate magnetometers. IEEE Trans. Magn. **8**(2), 223–231 (1972)
11. M. Butta et al., Influence of magnetostriction of NiFe electroplated film on the noise of fluxgate. IEEE Trans. Magn. **50**(11), 1–4 (2014)
12. P. Ripka, M. Pribil, M. Butta, Fluxgate Offset Study. IEEE Trans. Magn. **50**(11), 1–4 (2014)
13. F. Primdahl et al., Demagnetising factor and noise in the fluxgate ring-core sensor. J. Phys. E: Sci. Instrum. **22**(12), 1004 (1989)
14. R.H. Koch, J.R. Rozen, Low-noise flux-gate magnetic-field sensors using ring-and rod-core geometries. Appl. Phys. Lett. **78**(13), 1897–1899 (2001)
15. C. Moldovanu et al., The noise of the Vacquier type sensors referred to changes of the sensor geometrical dimensions. Sens. Actuators A **81**(1), 197–199 (2000)
16. O.V. Nielsen et al., Analysis of a fluxgate magnetometer based on metallic glass sensors. Meas. Sci. Technol. **2**(5), 435 (1991)
17. P. Ripka, Race-track fluxgate sensors. Sens. Actuators, A **37**, 417–421 (1993)
18. H.U. Auster et al., in *The THEMIS fluxgate magnetometer*. The THEMIS Mission (Springer, New York, 2009), pp. 235–264
19. O. Dezuari et al., Printed circuit board integrated fluxgate sensor. Sens. Actuators, A **81**(1), 200–203 (2000)
20. J. Kubik, M. Janosek, P. Ripka, Low-power fluxgate sensor signal processing using gated differential integrator. Sens. Lett. **5**(1), 149–152 (2007)
21. O. Zorlu, P. Kejik, W. Teppan, A closed core microfluxgate sensor with cascaded planar FeNi rings. Sens. Actuators A **162**(2), 241–247 (2010)
22. J. Lei, C. Lei, Y. Zhou, Micro fluxgate sensor using solenoid coils fabricated by MEMS technology. Meas. Sci. Rev. **12**(6), 286–289 (2012)
23. E. Delevoye et al., Microfluxgate sensors for high frequency and low power applications. Sens. Actuators A **145**, 271–277 (2008)
24. P. Butvin et al., Field annealed closed-path fluxgate sensors made of metallic-glass ribbons. Sens. Actuators A Phys. **184**, 72–77 (2012)
25. M. Janosek et al., Effects of core dimensions and manufacturing procedure on fluxgate noise. Acta Phys. Pol. A **126**(1), 104–105 (2014)
26. M.H. Acuna, Fluxgate magnetometers for outer planets exploration. IEEE Trans. Magn. **10**, 519–523 (1974)
27. K. Shirae, Noise in amorphous magnetic materials. IEEE Trans. Magn. **20**(5), 1299–1301 (1984)
28. D. Rühmer et al., Vector fluxgate magnetometer for high operation temperatures up to 250 °C. Sens. Actuators A Phys. **228**, 118–124 (2015)
29. A. Matsuoka et al., Development of fluxgate magnetometers and applications to the space science missions. Sci. Instrum. Sound. Rocket Satell. (2012)
30. O.V. Nielsen et al., Development, construction and analysis of the "Oersted" fluxgate magnetometer. Meas. Sci. Technol. **6**(8), 1099 (1995)

31. R. Piel, F. Ludwig, M. Schilling, Noise optimization of racetrack fluxgate sensors. Sens. Lett. **7**(3), 317–321 (2009)
32. F. Primdahl et al., The short-circuited fluxgate output current. J. Phys. E Sci. Instrum. **22**(6), 349 (1989)
33. B. Andò et al., in *Experimental investigations on the spatial resolution in RTD-fluxgates*. IEEE Instrumentation and Measurement Technology Conference, 2009 (IEEE 2009), pp. 1542–1545
34. D. High, Sensor Signal Conditioning IC for Closed-Loop Magnetic Current Sensor (Texas Instruments, 2006)
35. P. Ripka, W.G. Hurley, Excitation efficiency of fluxgate sensors. Sens. Actuators A **129**(1), 75–79 (2006)
36. J. Piil-Henriksen et al., Digital detection and feedback fluxgate magnetometer. Meas. Sci. Technol. **7**(6), 897 (1996)
37. W. Magnes et al., in *Magnetometer Front End ASIC*. Proceedings of 2nd International Workshop on Analog and Mixed Signal Integrated Circuits for Space Applications, (Noordwijk, 2008) pp. 99–106
38. C.T. Russell et al., The magnetospheric multiscale magnetometers. Space Sci. Rev. 1–68 (2014)
39. D.T. Germain-Jones, Post-war developments in geophysical instrumentation for oil prospecting. J. Sci. Instrum. **34**(1), 1 (1957)
40. W.L. Webb, Aircraft navigation instruments. Electr. Eng. **70**(5), 384–389 (1951)
41. S.F. Singer, in *Measurements of the Earth's Magnetic Field from a Satellite Vehicle*. Scientific uses of earth satellites (Univ. Michigan Press, Ann Arbor,1956), pp. 215–233
42. M.H. Acuna et al., in *The MAGSAT Vector Magnetometer: a Precision Fluxgate Magnetometer for the Measurement of the Geomagnetic Field*. NASA Technical Memorandum (1978)
43. T.J. Sabaka et al., CM5, a pre-Swarm comprehensive geomagnetic field model derived from over 12 yr of CHAMP, Ørsted, SAC-C and observatory data. Geophys. J. Int. **200**(3), 1596–1626 (2015)
44. Y.H. Pei, H.G. YEO, in *UXO Survey Using Vector Magnetic Gradiometer on Autonomous Underwater Vehicle*. OCEANS 2009, MTS/IEEE Biloxi-Marine Technology for Our Future: Global and Local Challenges (2009), pp. 1–8
45. F. Ludwig et al., Magnetorelaxometry of magnetic nanoparticles with fluxgate magnetometers for the analysis of biological targets. J. Magn. Magn. Mater. **293**(1), 690–695 (2005)
46. J. Tomek et al., Application of fluxgate gradiometer in magnetopneumography. Sens. Actuators A **132**(1), 214–217 (2006)
47. T. Kudo, S. Kuribara, Y. in *Takahashi, Wide-range ac/dc Earth Leakage Current Sensor Using Fluxgate with Self-excitation System*. IEEE Sensors (2011), pp. 512–515
48. Y. Nishio, F. Tohyama, N. Onishi, The sensor temperature characteristics of a fluxgate magnetometer by a wide-range temperature test for a Mercury exploration satellite. Meas. Sci. Technol. **18**(8), 2721 (2007)
49. J. Jeng, J. Chen, C. Lu, Enhancement in sensitivity using multiple harmonics for miniature fluxgates. IEEE Trans. Magn. **48**(11), 3696–3699 (2012)
50. J.M.G. Merayo, P. Brauer, F. Primdahl, Triaxial fluxgate gradiometer of high stability and linearity. Sens. Actuators A **120**(1), 71–77 (2005)
51. G. Sulzberger et al., in *Demonstration of the Real-time Tracking Gradiometer for Buried Mine Hunting while Operating from a Small Unmanned Underwater Vehicle*. IEEE Oceans (2006)
52. Y. Sui et al., Compact fluxgate magnetic full-tensor gradiometer with spherical feedback coil. Rev. Sci. Instrum. **85**(1), 014701 (2014)
53. M. Kashmiri et al., in *A 200kS/s 13.5 b Integrated-fluxgate Differential-magnetic-to-digital Converter with an Oversampling Compensation Loop for Contactless Current Sensing*. IEEE International Solid-State Circuits Conference-(ISSCC), 2015 (IEEE, 2015), pp. 1–3

54. Texas Instruments Inc., DRV425—Fluxgate Magnetic-Field Sensor (2015), http://www.ti.com/lit/ds/symlink/drv425.pdf
55. A. Cerman et al., in *Self-compensating Excitation of Fluxgate Sensors for Space Magnetometers.* IEEE Instrumentation and Measurement Technology Conference Proceedings, 2008 (IEEE, 2008), pp. 2059–2064
56. K.-H. Glassmeier et al., RPC-MAG the fluxgate magnetometer in the ROSETTA plasma consortium. Space Sci. Rev. **128**(1–4), 649–670 (2007)